Mineralogical, petrographic and physical-mechanical study of Roman construction materials from the Maritime Theatre of Hadrian's Villa (Rome, Italy)

S. Columbu[a,*], C. Lisci[a], F. Sitzia[a], G. Lorenzetti[b], M. Lezzerini[c], S. Pagnotta[b,c], S. Raneri[c], S. Legnaioli[b], V. Palleschi[b], G. Gallello[d], B. Adembri[e]

[a] Department of Chemical and Geological Sciences, University of Cagliari, Via Trentino, 51 – 09127 Cagliari, Italy
[b] Institute of Chemistry of Organometallic Compounds, Applied and Laser Spectroscopy Laboratory, Research Area of National Research Council, Via G. Moruzzi, 1 – 56124 Pisa, Italy
[c] Department of Earth Sciences, University of Pisa, Via Santa Maria, 53 – 56126 Pisa, Italy
[d] Department of Archaeology, University of York, King's Manor, York YO17EP, UK
[e] Istituto Autonomo Villa Adriana e Villa d'Este, Ministero dei Beni e delle Attività Culturali e del Turismo, Piazza Trento, 5 – 00019 Tivoli, Roma, Italy

ABSTRACT

This paper presents the study of various Roman materials used in the construction of the Maritime Theatre, one of the main buildings in the Hadrian's Villa complex, a designated UNESCO World Heritage Site located in Tivoli (Rome, Italy), dating to the first half of the II century A.D. The plaster layers (*arriccio* and *intonachino*) and overlying original Roman paintings that form the concave wall of the *portico* as well as some bedding mortars of the pyramidal stone elements (*i.e. cubilia*) of the circular masonry have been studied in particular. In addition, the acid volcanic rocks of the *cubilia* have been investigated, aiming to understand their state of alteration and geological origin.

By mineralogical-petrographic microscopy (OM), diffractometry (XRPD), Raman spectroscopy, Point Load Tests (PLT), helium pycnometry, and particle size analysis, the composition and granulometric distribution of the aggregate, type and characteristics of the binder, and various physical-mechanical properties (density, porosity, water absorption, imbibition and saturation indices, mechanical resistance) of mortars and stones were defined. In addition, through digital image analysis of thin sections, the binder/aggregate ratio and some geometric characteristics of the aggregates (*e.g.* circularity) were determined.

The research aims to improve the knowledge of the constructive technologies of the Maritime Theatre through the analysis of its materials.

1. Introduction

The Maritime Theatre (Fig. 1) is one of the most important buildings within Hadrian's Villa [1,2], which dates to the II century A.D. and has been a UNESCO World Heritage Site since 1999. The theatre embodies the uniqueness and innovative design of the entire residential complex. Its name comes from the subject of the marble trabeation of the inner peristyle, which is decorated with a sea procession of the Erotes and other mythological figures carved in a very refined style. This place was a sort of secret study devoted to meditation, cultural and leisure activities. Partially inaccessible since 2010 as a consequence of earthquake damage, it has recently been restored (2014–2017) and is now accessible by visitors.

The structure of the building (Figs. 1 and 2) consists of a circular body preceded by a *pronaos* that enters an annular *portico* supported by Ionic columns and covered by a barrel vault. The colonnade, reflected in the water of a large internal channel, surrounds an artificial island which was accessible via two wooden swing bridges. The island is an effective miniature villa within the Imperial residence, a luxurious and comfortable space which has been optimally designed to meet all the needs of the Emperor. The scheme of the internal environments, albeit reduced and conditioned by the circular plan, reiterates in its constitutive elements the typical one of the *domus*, with *atrium*, inner courtyard, *portico* for walking, *tablinum*, *cubicula*, thermal baths and even three toilets.

Hadrian's Villa has been the subject of several archaeological and

---

* Corresponding author.
  E-mail address: columbus@unica.it (S. Columbu).

Fig. 1. The Maritime Theatre: (a) the central island, (b) the circular canal, (c) ruins of the inner portico with figured trabeations, (d) ruins of barrel-vault support column, (e) building ruins on the island, (f) circular corridor with a small stretch of barrel-vault cover, (g) digital representation of plan and section according to the hypothesis by Üblacker (elab. E. Cozzato), (h) isometric representation of Üblacker's hypothesis (wire-frame).

architectural studies [1–8]. Some of these were also on the characterization of raw materials, especially the marbles of various colours, used in the floors and walls, and their origin from the Mediterranean ancient quarries [9–14].

This research aims to characterize the Roman mortars and the pyramidal volcanic stone elements (*i.e. cubilia*) used in the construction of the Maritime Theatre. The layers (*arriccio* and *intonachino*) of some

plasters and paintings from the concave wall of the *portico* and bedding mortars of the *cubilia* of the circular weight bearing masonry have been especially investigated. The purpose is to develop understanding of the constructive technologies [15,16] used at the Maritime Theatre through the identification of the building materials. The specific aims are to define: i) the composition and distribution of the aggregate, type and characteristics of the binder, and various physical-mechanical
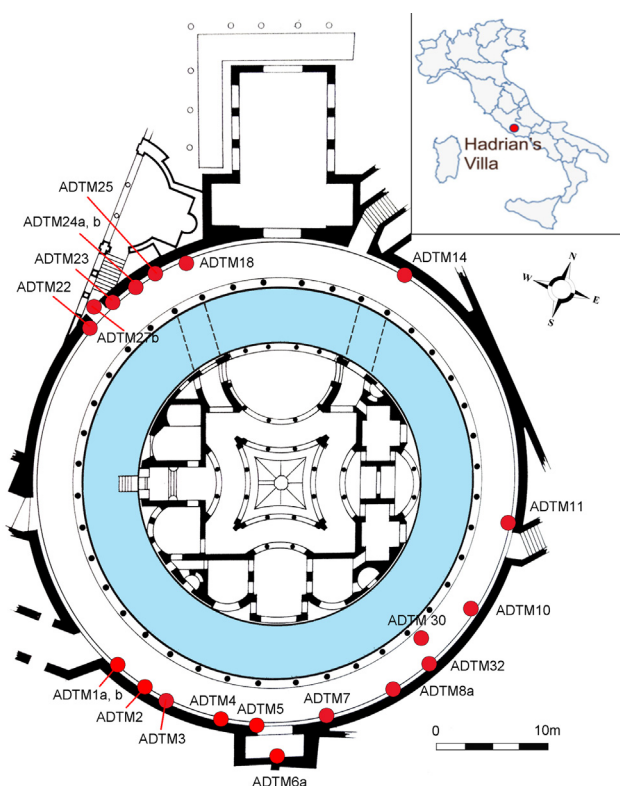
Fig. 2. Sampling archive map of Maritime Theatre Roman building.

properties of mortars, namely density, porosity, water absorption, imbibition and saturation indexes, and mechanical resistance, by mineralogical-petrographic microscopic (OM), XRPD analysis, water/helium pycnometry and Point Load Testing (PLT) respectively; ii) the binder/aggregate ratio and some geometric characteristics of the aggregates (*e.g.* circularity of fragments) by thin section digital image analysis; and iii) the composition of the coloured layers of some painting mortar samples from the *portico* wall and the raw materials used in the pigments, by Raman analysis. In addition, the petrographic characteristics of *cubilia* elements made with acid volcanic rocks have been studied, aiming to understand their state of alteration and geological origin.

The geochemical, mineralogical, petrographic and physical characterization of ancient geomaterials is very useful in defining the compositional standards of mortars in relation to their function in the monument, their technical quality and any heterogeneity resulting from the production process, the construction phases of the building, the origin of stones utilized and the alteration processes [17–39].

2. Material and methods

Twenty-one samples were taken from the monument and analysed (Table 1) of which 8 were brick bedding mortars (Fig. 3a and b), 5 *cubilia* bedding mortars (Fig. 3c and d), 2 renderings (*i.e. arriccio* layers, Fig. 3e and f), 2 setting coat plasters (*i.e. intonachino* layers, Fig. 3 g and h), 4 *cubilia* pyroclastics (Fig. 3i and l).

Macroscopic characteristics (in Table 1) are reported as alteration degree, binder flaw and binder colouring coordinates according to CIELAB colour space.

Petrographic determinations of mineralogical composition and modal analysis of mortars were carried out by optical polarised microscopy on polished thin sections.

The binder/aggregate ratio (B/A) of mortars was calculated through image analysis (by ImageJ 1.47v) on thin section photographs detected with a flatbed scanner.

A Seifert X3000 apparatus in the Bragg–Brentano geometry was

used for X-ray Powder Diffraction (XRPD). It was operated using the CuKα radiation in the range of 8–40 (2θ degrees) with step of 0.05 2θ, with an opportune counting time to optimize the signal/noise ratio. JCPDF-2 database was used for the identification of the phases. Raman spectroscopy was used to investigate the chemical components and pigments present in the painting samples. These analyses were carried out at the Applied Laser Spectroscopy Laboratory of the Institute of Chemistry of Organometallic Compounds, ICCOM-CNR U.O.S. of Pisa. A Renishaw Raman inVia instrument equipped with a Leica microscope with 50× lens was used, with the diffraction reticle set at 1800 line/mm and a CCD detector. The choice of laser sources to be used, based on the sample to be analysed, was between a HeNe laser (λ = 633 nm) and a Nd: YAG (λ = 532 nm).

Physical tests were performed according to different methods [40] on cubic specimens with edge of 15 (± 5) mm dried at 105 ± 5 °C and then the dry solid masses (m_D) were determined. The real volume was calculated as:

$$V_R = V_S + V_C \tag{1}$$

where: V_C is the volume of closed pores to Helium; V_S is the volume of solid fraction. V_C was determined by helium pycnometer (Ultra-pycnometer 1000 model of Quantachrome Instruments).

Then, the wet solid mass (m_W) of the samples was determined after water absorption by immersion for 10 days. Through a hydrostatic analytical balance, the bulk volume V_B with:

$$V_B = V_S + V_O + V_C \tag{2}$$

where $V_O = (V_B - V_R) \tag{3}$

is the volume of open pores to helium. V_B is calculated as:

$$V_B = ((m_W - m_{HY})/\rho_w T_{25°C})100 \tag{4}$$

where m_{HY} is the hydrostatic mass of the wet specimen and ρ_{WTX} is the water density (0.9970 g/cm³) at 25 °C.

Total porosity (Φ_T), open porosity to water and helium ($\Phi_O H_2O$, $\Phi_O He$ respectively), closed porosity to water and helium ($\Phi_C H_2O$; $\Phi_C He$), bulk density (ρ_B), real density (ρ_R), solid density (ρ_S), were computed as:

$$\Phi_T(\%) = [(V_B - V_S)/V_B]100 \tag{5}$$

$$\Phi_O H_2O(\%) = [(m_W - m_D)/\rho_{WT25°C}]/V_B)100 \tag{6}$$

$$\Phi_C H_2O(\%) = \Phi_T - \Phi_O H_2O \tag{7}$$

$$\Phi_C He(\%) = \Phi_T - \Phi_O He \tag{8}$$

$$\rho_S = m_D/V_S(g/cm^3) \tag{9}$$

$$\rho_R = m_D/V_R(g/cm^3) \tag{10}$$

$$\rho_B = m_D/V_B(g/cm^3) \tag{11}$$

Weight imbibition coefficient (IC_W) and the saturation index (SI) were computed as:

$$IC_W(\%) = ((m_W - m_D)//m_D)100 \tag{12}$$

$$SI(\%) = (\Phi_O He/\Phi_O H_2O)100 \tag{13}$$

Punching strength index was determined with a Point Load Tester (mod. Controls D550 Instrument) in accordance with the ISRM Recommendations [41,42] on the same pseudo-cubic specimens used for other physical properties (porosity, density, water absorption, etc.). The load was exerted via the application of a concentrated load with two opposing conical punches. The resistance to puncturing (Is) was calculated as:

$$P/D_e^2(N/mm^2) \tag{14}$$

where P (N) is the breaking load and D_e is the "equivalent diameter of the cylindrical sample" [42], with
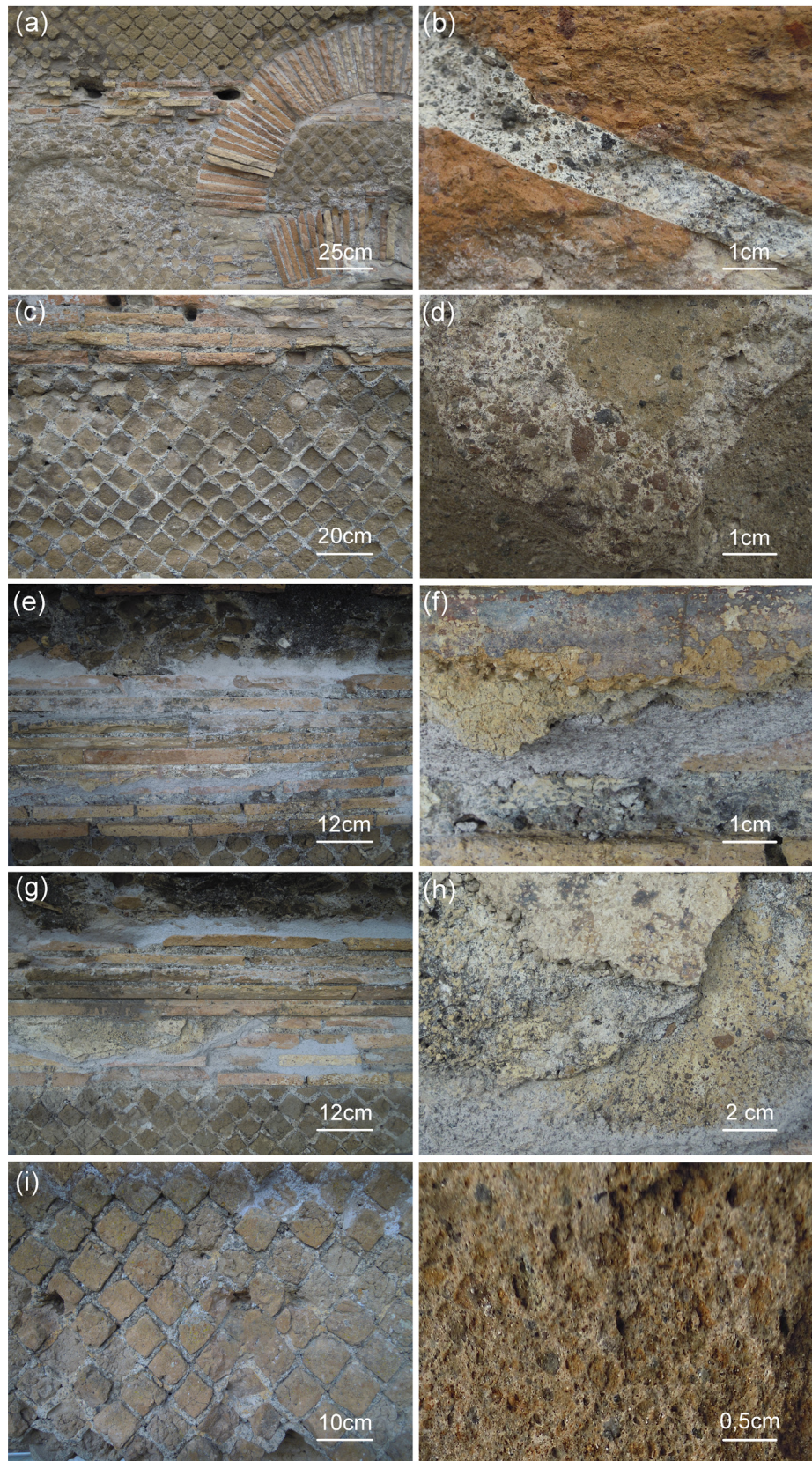
Fig. 3. Sampling with macroscopic features: (a,b) brick bedding mortars (sample ADTM1a), (c,d) *cubilia* bedding mortars (sample ADTM3), (e,f) rendering (sample ADTM24a), (g,h) detail of setting coat plaster (sample ADTM25) taken from the inner concave wall under the *portico* vault, belong to the original painting consisting of two different coloured levels, (i,l) *cubilia* pyroclastites (sample ADTM27).

Table 1
Sampling Log.

Sample	Mortar/lithology type	Alteration, binder flaw	Binder colouring (CIELAB)
ADTM 1a	Brick-bedding mortars	Binder dissolution with aggregate enucleation and presence of lime lumps	81*-1*-5
ADTM 2			79*-1*3
ADTM 4			84*-1*3
ADTM 5			82*-1*4
ADTM 6a			72*0*5
ADTM 8a			72*1*3
ADTM 10			72*1*4
ADTM 11			72*-1*3
ADTM 3	*Cubilia* bedding mortars	Binder dissolution with aggregate enucleation and presence of lime lumps	79*0*4
ADTM 7			61*1*3
ADTM 14			80*-2*4
ADTM 22			66*-1*4
ADTM 23			72*0*2
ADTM 24a	Renderings (*arriccio*)	Material defect	70*-1*15
ADTM 32			82*1*2
ADTM 24b	Setting coat plasters (*intonachino*)	Material defect	70*-1*13
ADTM 25			70*-1*8
ADTM1b	*Cubilia* pyroclastites	Decohesion, flaking, exfoliation	44*0*13
ADTM18			50*1*9
ADTH27b			48*1*12
ADTM30			53*0*15

$$D_e^2 = 4A/P (mm^2) \qquad (15)$$

$$A = WD (mm^2) \qquad (16)$$

where W and D are the width perpendicular to the direction of the load and the length of the specimen respectively. The index value is compared to a standard cylindrical specimen with diameter D = 50 mm for which Is has been corrected with a shape coefficient (F) and calculated as:

$$Is_{(50)} = Is \ F = Is(D_e/50)^{0,45} \qquad (17)$$

The simple compression resistance (R_C) and the traction resistance (R_T) of the mortar were indirectly calculated (according to ISRM 1985) using the value of normalized punching resistance, with each of them as:

$$R_C = K \ Is_{(50)} \qquad (18)$$

$$R_T = Is_{(50)}/0.8 \qquad (19)$$

where K (multiplication coefficient) = 14 [43].

For the particle size analysis, the mortars were first disaggregated with the use of a mortar and pestle, dried at 105 ± 5 °C, weighed to measure the dry mass (m_{dM}), and then attacked with an acid solution (HCl, 13% vol.) for an immersion period of 48 h, so as to eliminate the carbonate binder matrix of the mortar. The samples were then filtered with Whatmann 41 paper, washed in distilled water, placed in an oven at 105 ± 5 °C to determine the dry mass of the residual aggregate (m_{dR}) and, indirectly, the bulk mass of the binder (as: $m_{dB} = m_{dM}$-m_{dR}). Then, the particle size distribution was performed using sieve series UNI 2131, with mesh opening of 6300, 4000, 2000, 500, 250, 125, 63 μm with a Giuliani IG/3 sifter.

3. Results and discussion

To better define Roman construction technologies, in the following discussion the data for the mortars and stones sampled from the Maritime Theatre (here called MT) were compared with data of the geomaterials of the nearby *Heliocaminus* Baths (one of the three Baths in Hadrian's Villa; here called HB) studied by Columbu *et alii* [9–11].

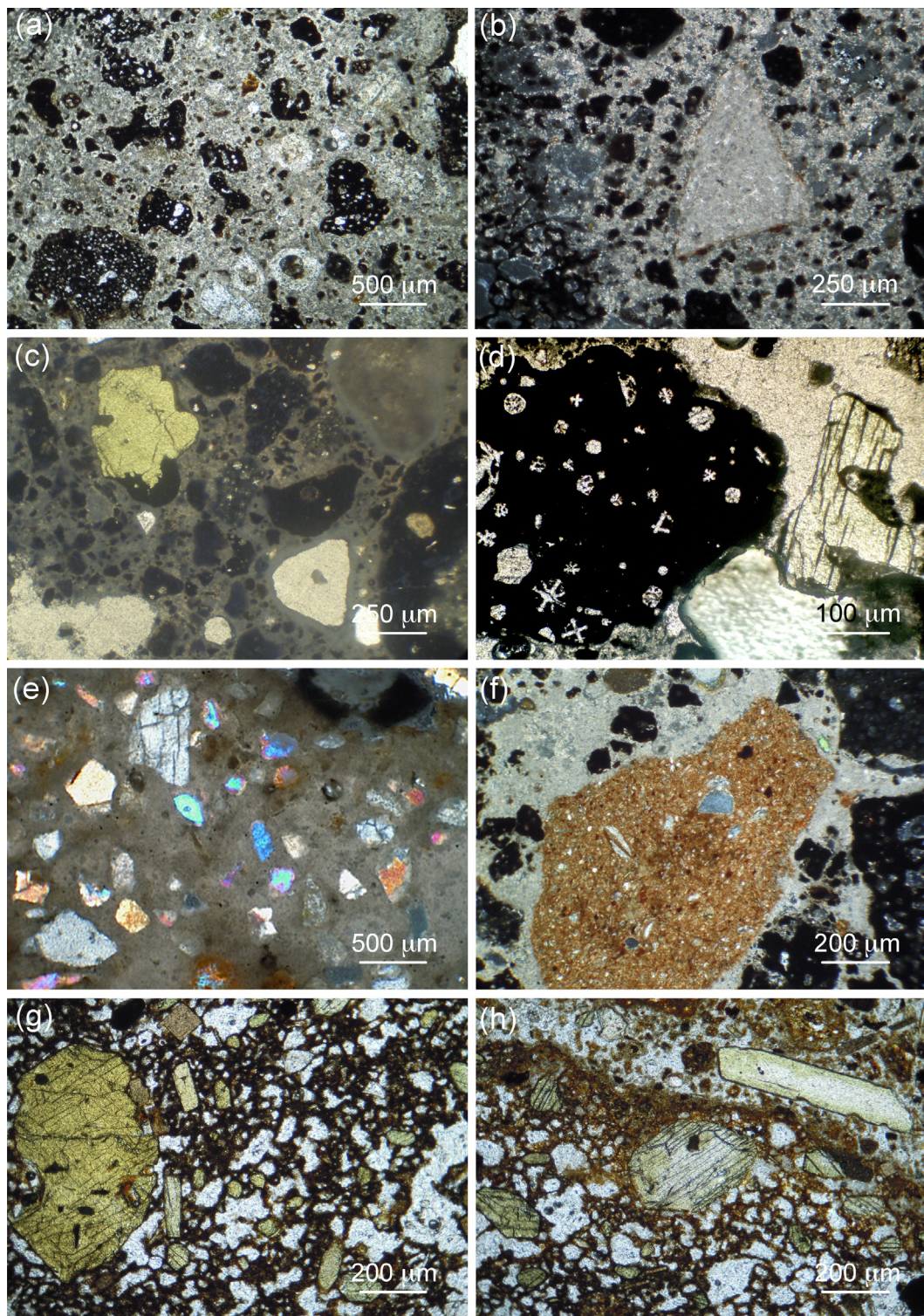### 3.1. Composition, mineralogical and petrographic features

Macroscopic observations (Table 1) and microscopic modal analysis in thin section (Table 2) allowed the characterization of the studied mortars' aggregate composition, binder reactivity with the aggregate, and the presence of lime lumps.

In MT bricks and *cubilia* bedding mortars and renderings, the binder has colours ranging from light grey to whitish on freshly cut mortar specimens (Fig. 3a–d) according to space colour CIELAB (Table 1). In some cases, on the external exposed surfaces, due to the weathering, the samples show more intense colours up to grey.

In the case of renderings and setting coat plasters (samples ADTM24a, 32, 24b, 25), a yellowish colour characterizes the samples due to deep penetration of the painting's pigments (Table 1, Fig. 3e–h).

In all mortars, the binder frequently shows the presence of sub-circular lime lumps with dimensions from sub-millimetre to 10 mm. Biological patinas are sometimes present with colour from grey-black (*e.g.* moulds) to light green to white to yellow (*e.g.* mosses, lichens).

The mortars' aggregate is composed of two main kinds of volcanic rocks (*i.e.* leucitic basalts and leucitites; Fig. 4a and d), crystal clasts (*i.e.*

Table 2
Modal analysis with percentage of different aggregates present in the analysed mortars.

Sample	Mortar type	Rock fragments (%)			Crystal-clasts (%)				Total aggregate (%)
		Scorias	Leucitite	*Cocciopesto*	Marble	Cpx	Hnb	Bt	
ADTM 1a	Brick bedding mortars	97	1.5	0	0	0.5	1	0	100
ADTM 2		99.3	0.2	0.5	0	0	0	0	100
ADTM 4		98	1	0	0	0.5	0.5	0	100
ADTM 5		96.2	3.2	0	0	0.4	0.2	0	100
ADTM 6a		98.4	1	0.1	0.2	0.3	0	0	100
ADTM 8a		97.5	1	0	0	1	0.5	0	100
ADTM 10		98	1	0	0.2	0.8	0	0	100
ADTM 11		97.5	2	0	0.5	0	0	0	100
ADTM 3	*Cubilia* bedding mortars	98.8	1.2	0	0	0	0	0	100
ADTM 7		98.5	1	0	0	0.5	0	0	100
ADTM 14		95.8	2	0	0	0.5	1	0.7	100
ADTM 22		98	0.5	0	0.2	0.6	0.7	0	100
ADTM 23		97	2	0.3	0	0.2	0.5	0	100
ADTM 24a	Renderings (*arriccio*)	96.0	0	0.1	0	0.5	3.2	0.2	100
ADTM 32		96.3	0	0.1	0	0.2	3.0	0.4	100
ADTM 24b	Setting coat plasters (*intonachino*)	1	0	0.2	0	95.8	2.8	0.2	100
ADTM 25		1	1	0.1	0	95.5	2.2	0.2	100

Fig. 4. Microscopic features: (a) scoria black aggregates in brick bedding mortars ADTM1a, (b) marble fragment in *cubilia* bedding mortars ADTM22, (c) clinopiroxene and green Hornblende crystal-clasts in cubilia bedding mortars ADTM14, (d) leucitite aggregate in Brick bedding mortars ADTM5, (e) crystal-clasts aggregate in renderings ADTM24b (crossed Nicol), the plasters have high binder/aggregate ratios, well-blended, indicating a particular care in making mortar considered its technical function as support for mural painting, where the volcanic aggregate is well-classed (unimodal distribution, with predominantly fine granulometry mostly composed of crystalloclasts), (f) *cocciopesto* fragment aggregate in sample ADTM25, (g,h) *cubilia* with green hornblende phenocrysts.

single crystalline phases; Fig. 4c and e), rare *cocciopesto* fragments (crushed bricks, tiles and pottery; Fig. 4f) and rare marble fragments (Fig. 4b). The analysed mortars show a similar composition of aggregates to the HB mortars.

In MT bricks and *cubilia* bedding mortars and renderings, the

aggregate is mainly represented by leucitic basalt (as scoria) with a frequency of 97.5% with respect to the total aggregate (Table 2). It shows great similarity with volcanic scoria outcropping at several locations near Hadrian's Villa. This aggregate has predominantly sub-spherical shapes and a colour from grey-red or grey-black and

belonging to the alkaline rocks of the ultrapotassic series (HKS) of the Roman Magmatic Province [44]. The leucitic basalt appears vitreous and porous, with aphyric texture. The paragenesis is composed of clinopyroxene, leucite, green hornblende, opaque minerals and rare plagioclase, immersed in a glassy groundmass. Rare crystals of biotite and olivine (the latter often altered into iddingsite) are present. The leucitic basalt aggregate shows the edges of pozzolanic reaction with the binder. In these brick and *cubilia* bedding mortars, crystal clast aggregate is rare or, in some case, absent.

In contrast, in setting coat plasters, the aggregate is mainly represented by crystal clasts (about 98–99% of the total; Table 2) with rare scoria fragments (about 1%). In this group, crystal clasts are represented by clinopyroxene (95.7% of total aggregate), green hornblende (2.5%) and rare biotite (Table 2).

In all groups of mortars, the *cocciopesto* aggregate is rare to absent but it presents (probably as accidental fragments) in very low percentages (from 0.1% in renderings and setting coat plasters to 0.5% in brick bedding mortars). *Cocciopesto* shows a variable colour from yellow ochre to pink-orange to rust red. The fragments of this aggregate often have an angular shape with variable physical characteristics (porosity, size, etc.) and compositions. It shows clear edges of reaction with the binder.

Crystal clasts are immersed in the micrometric matrix and they mainly consist of quartz and plagioclase. Rarely, even fragments of leucitic basalts (about 3% on the total of thin section) are found. Phases of iron oxides (*e.g.* hematite) are also present. The marble aggregate is randomly found in small percentages in the matrices of some bricks and *cubilia* bedding mortar samples.

A comparison between MT mortars and HB mortars according to the classification group shows, as mentioned earlier, the same aggregate components. It also results in the same relative aggregate percentages in the groups [11], where bricks and *cubilia* bedding mortars and renderings present a large amount of scoria (95.1% of total aggregate), a small amount of crystal clasts (1.1% of total aggregate) and the absence of *cocciopesto*.

Raman spectroscopic analysis of two painting layers (reddish and dark-brown; Fig. 3e–h) taken from the wall plasters (*intonachino* layers) located under the vault was carried out at different points and microstratigraphic levels of the samples. The analysis on the reddish level highlights a spectrum typical of hematite with peaks on 225, 244, 292, 410 e 612 cm^{-1} (Fig. 5a).

The dark-brown zone was analysed using a Nd: YAG laser (λ = 532 nm). From the analyses, it is made up of Egyptian blue with characteristic peaks on 117, 133, 190, 225, 375, 427, 465, 565, 760, 785, 980, 1004 and 1080 cm^{-1} (Fig. 5b).

The stone used for the *cubilia* small pyramidal ashlars (with the side of the square base about 7 cm) is a pyroclastic rock. Given its medium–low welding, it mainly shows evident physical degradation due to decohesion, flaking and exfoliation processes. It is characterized by a glassy groundmass (Fig. 4h) occasionally with typical alterations into zeolites and clay minerals [44], where lithic clasts of varying particle size, with composition from leucitic basaltic to leucititic, and xenoliths are present. The accessory phases are iron and titanium oxides. By microscopic observations with parallel Nicols, they have a reddish colour or, only rarely, grey-black.

From a thin section comparison of volcanic tuff with samples of pyroclastics collected inside Hadrian's Villa, it is suggested that the volcanic material used to make the *cubilia* was extracted from nearby outcrops. *Cubilia* pyroclastics of the Maritime Theatre are similar to those used at the *Heliocaminus* Baths. As in the latter site, these volcanic materials were also used as pozzolan or simple aggregate in the mortars (and probably also as a component in the bricks). In fact, the presence of the same crystal clasts observed in the pyroclastics has been frequently detected (*i.e.* green hornblende, clinopyroxene, biotite) as well as the presence of leucitic basalts and leucitites.

3.2. Binder/aggregate ratio and particle size

By image analysis on thin section microphotographs, the binder/aggregate ratio of MT mortar groups was determined (Table 3). Four images of selected samples (for each group) are reported in Fig. 6a–d.

MT brick bedding mortars present binder/aggregate ratio values ranging from 0.15 (ADTM11) to 0.50 (ADTM5) with an average value 0.27 (Table 3), excluding the sample ADTM2 that shows a very small value. The same group of HB mortars shows a greater binder/aggregate ratio with a value of 0.83. The circularity average value of aggregates of this MT mortar group varies between 0.82 and 0.86 with a mean of 0.84.

MT *cubilia* bedding mortars have an average ratio value of 0.92, with high variability ranging from 0.30 (sample ADTM3, Fig. 6b) to 1.76 (ADTM14). The circularity average value of aggregates is 0.83. MT binder/aggregate ratios for *cubilia* bedding mortars (Fig. 6b, sample ADTM4) are similar to those of HB mortars (with a mean of 1.06), while the average circularity values are different between the two ancient buildings, with a value in HB mortars slightly lower (0.59) with respect to those from MT mortars.

On rendering samples ADTM24a and ADTM32, image analysis shows average binder/aggregate ratio values of 4.49 and 5.22 respectively (Table 3). The circularity values of their aggregates are 0.70 and 0.74. In *Heliocaminus* Baths, rendering samples ADTH13 and ADTH14
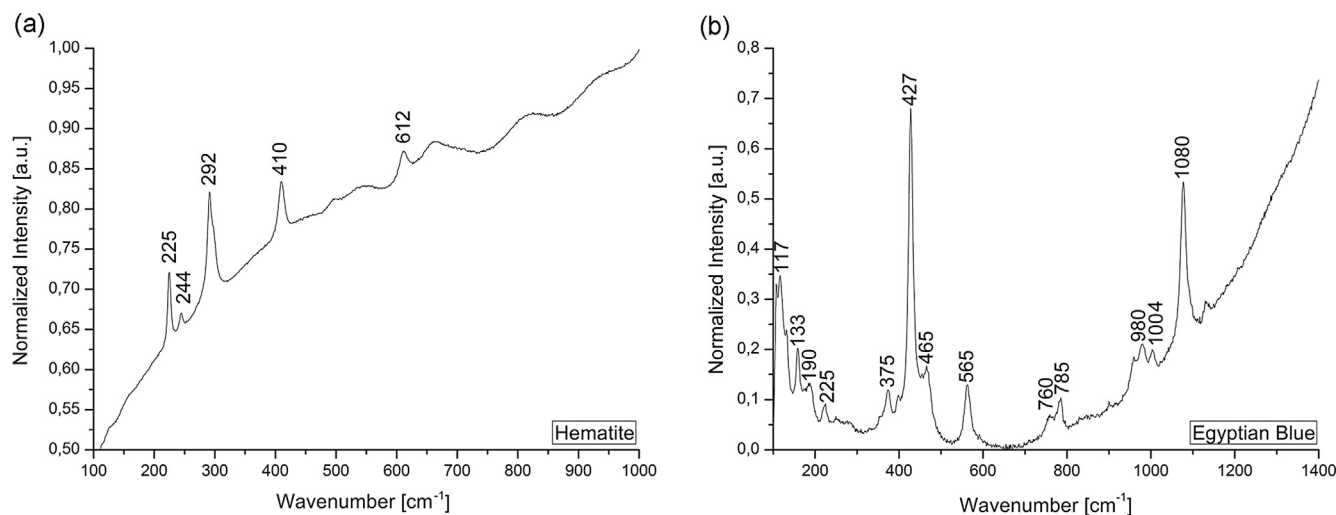

Fig. 5. Raman spectroscopy analysis of painting levels taken from the *intonachino* plasters (samples ADTM 24 and ADTM 25): (a) reddish level; (b) grey-black level.

Table 3
Image analysis on thin section microphotographs of mortar aggregate, where reported: circularity variation (minimum - maximum range), circularity average, mean of circularity average and binder/aggregate ratio (B/A).

Sample	Mortar type	Circularity variation (min – max)	Circularity average	Mean of circularity average	Standard deviation	B/A on thin section	Average B/A
ADTM 1a	Brick bedding mortars	0.06–1	0.84	0.84	0.21	0.28	0.27
ADTM 2		0.06–1	0.84			0.03	
ADTM 4		0.05–1	0.83			0.28	
ADTM 5		0.07–1	0.85			0.50	
ADTM 6a		0.02–1	0.84			0.41	
ADTM 8a		0.04–1	0.82			0.18	
ADTM 10		0.08–1	0.82			0.34	
ADTM 11		0.02–1	0.86			0.15	
ADTM 3	*Cubilia* bedding mortars	0.03–1	0.83	0.83	0.21	0.30	0.92
ADTM 7		0.10–1	0.84			0.59	
ADTM 14		0.06–1	0.82			1.76	
ADTM 22		0.04–1	0.82			0.87	
ADTM 23		0.02–1	0.83			1.09	
ADTM 24a	Renderings (*arriccio*)	0.07–1	0.70	0.72	0.22	4.49	4.86
ADTM 32		0.07–1	0.74			5.22	
ADTM 24b	Setting coat plasters	n.d.	n.d.	n.d.	n.d.	n.d.	n.d.
ADTM 25	(*intonachino*)	0.01–1	0.85			1.52	

have binder/aggregate ratio values of 0.87 and 1.02 respectively (Table 3) with circularity values of 0.56 and 0.58 respectively. Setting coat plaster sample ADTM25 shows a binder/aggregate ratio value of 1.52 and a circularity of 0.85 (Table 3).

Circularity differences between the two ancient buildings inside the same group are probably attributable to different supply facies of pozzolanic aggregates. Instead, different B/A ratios are attributable to differences in workforce and/or different times of construction. It is in fact known that the construction of Hadrian's Villa took place in three main phases from 118 to 121 CE.

The data from particle size analysis carried out on the aggregates of MT brick and *cubilia* bedding mortars are reported in Table 4 and the results of selected samples are shown in Fig. 7 (samples ADTM3 and ADTM11). In the mortars, hold masses centred on 4000 and 2000 μm sieve openings. The same results were recorded in HB brick and *cubilia* bedding mortars. The cumulative passing diagrams for both the MT mortar samples indicate gravelly-sandy aggregates with highly variable particle size (with a uniformity coefficient > 15). The particle grain
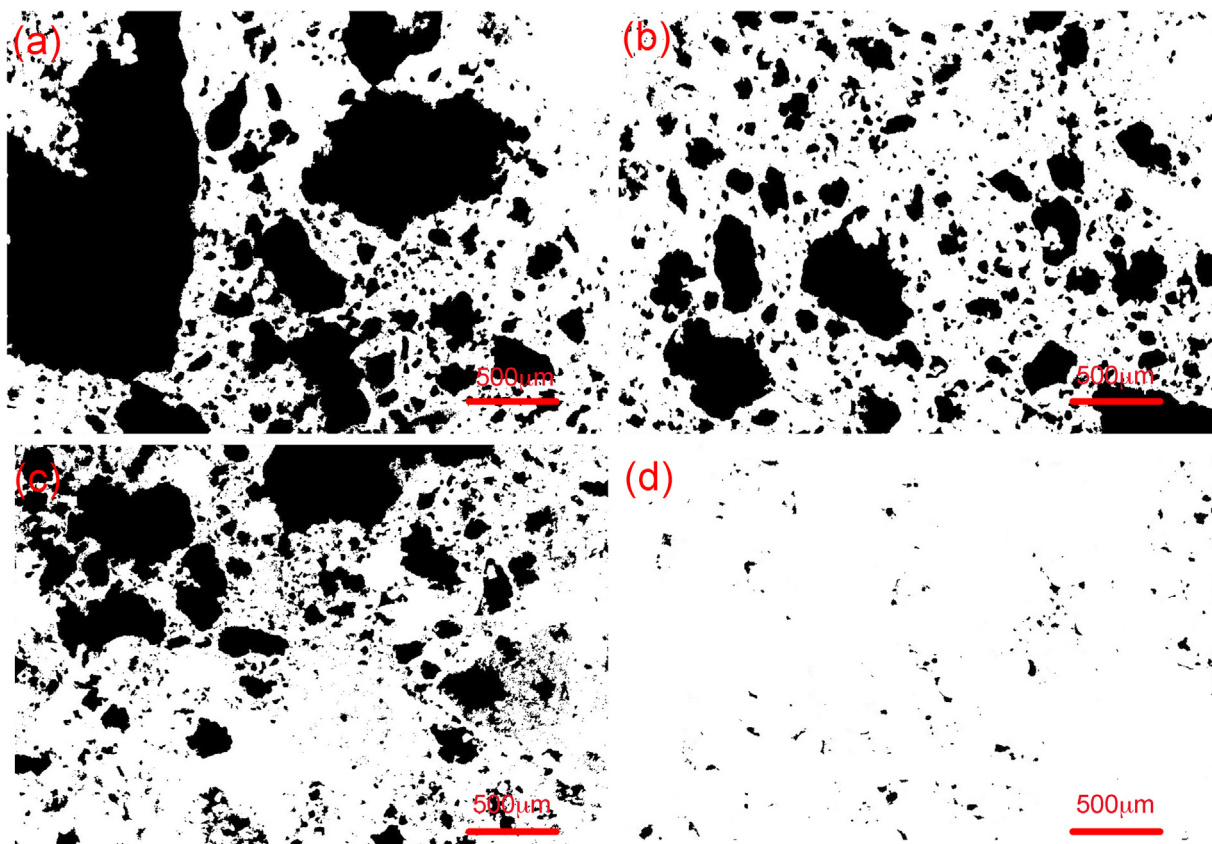

Fig. 6. Analysis on black-white binarized images: (a) brick bedding mortars (sample ADTM4), (b) *cubilia* bedding mortars (sample ADTM3), (c) rendering (sample ADTM32), (d) setting coat plaster (sample ADTM24b).

Table 4

Particle size analysis data, where reported hold mass and cumulative passing (%) according to the 8000, 4000, 2000, 1000, 500, 250, 125, 63, < 63 µm sieves.

Sample	Mortar type	Sieve diameter (µm)	8000	40,000	2000	1000	500	250	125	63	< 63
ADTM 3	*Cubilia* bedding mortars	Hold mass (%)	0	41.79	15.41	11.51	11.34	9.59	5.27	3.48	1.62
		Cumulative passing (%)	100	58.21	42.80	31.29	19.95	10.37	5.10	1.62	0
ADTM 11	Brick bedding mortars	Hold mass (%)	0	52.11	22.08	7.98	6.51	5.24	3.28	1.88	0.92
		Cumulative passing (%)	100	47.89	25.81	17.83	11.32	6.08	2.80	0.92	0
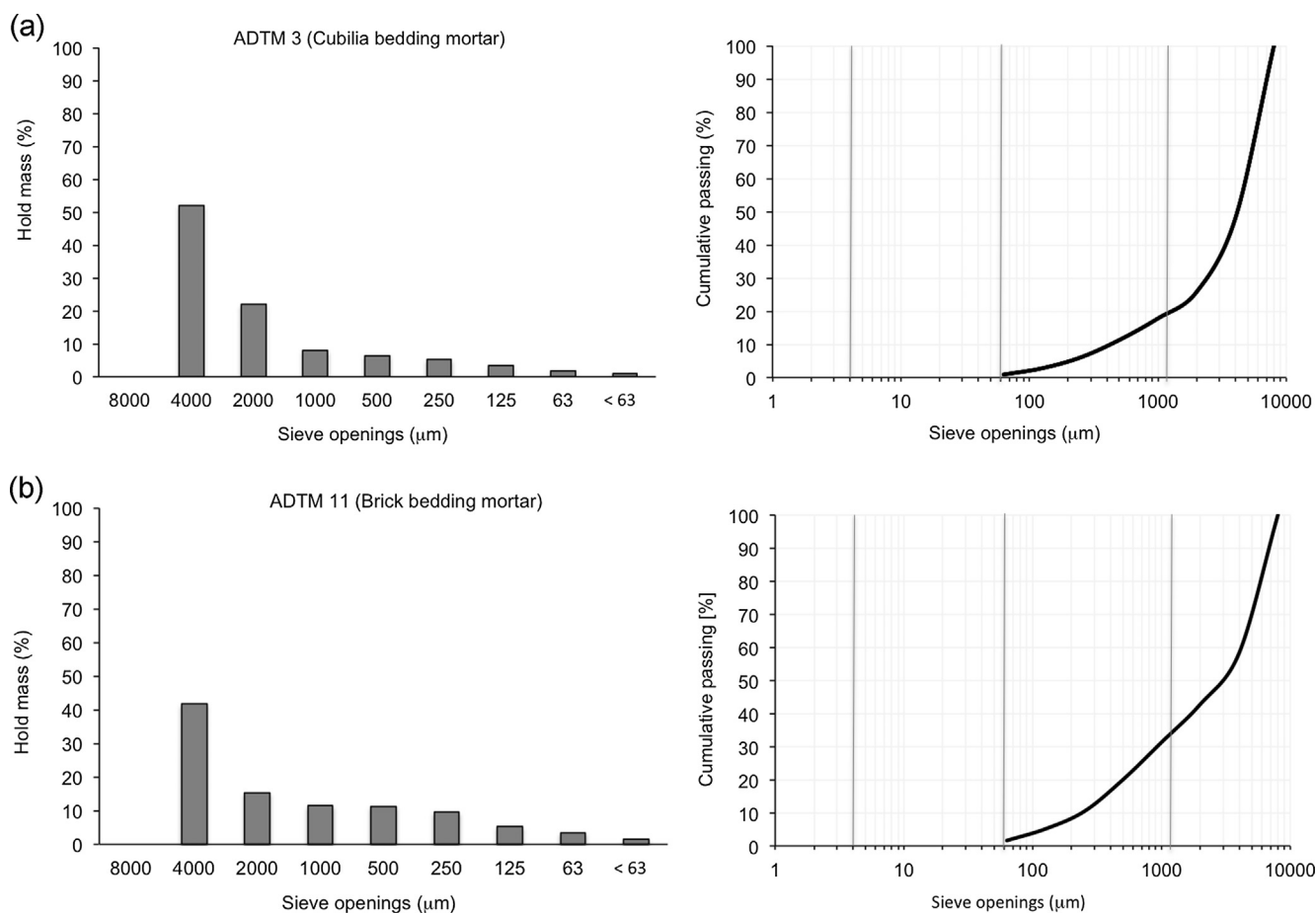
Fig. 7. Particle size analysis results of mortar aggregate: (a) *cubilia* bedding mortars (sample ADTM3), (b) brick bedding mortars (sample ADTM11).

size of aggregates and composition of these MT mortars reflects the same manufacturing technology used in *Heliocaminus* Baths and follows *Vitruvio*'s requirements [45], indicating a sorted aggregate for mortars that allows for lime savings and better mechanical resistance.

3.3. Physical and mechanical properties

For the sampled MT mortars and volcanic pyroclastics used for *cubilia* ashlars, the solid, real and bulk densities, open and closed porosity to helium and water, weight imbibition coefficient, saturation index, punching strength and indirect compression and traction strengths (Table 5 and 6) were the physical and mechanical properties determined.

Mortar samples show a wide variability of the physical properties (Table 5), due to the diversity of aggregate components (*i.e.* volcanic scoria, leucitite rock, *cocciopesto*) and the variable binder/aggregate ratio according to the function of mortar in the MT monument. Furthermore, the diverse characteristics of the binders affect the physical data, as a function of mortar manufacturing. In fact, according to the results of Columbu *et alii* [10,11] carried out on the HB mortars, the MT mortar binders have relatively high variability of open and closed

porosity.

Considering all analysed MT mortars, the helium open porosity ranges between about 30 and 48% and the bulk density between 1.28 and 1.77 g/cm^3 (Fig. 8a; Table 5). Despite this variability, a good linear correlation (Fig. 8a) between these two parameters is observed, showing that the bulk density mainly depends on the porosity and less on real density that is affected by the nature of the solid phases (crystalline or amorphous types). However, a good positive correlation is also observed between the bulk and real densities, as shown in the graph in Fig. 8b.

Observing Fig. 8a, a partial overlap between the MT and HB mortar samples can be seen. However, different values of these physical properties are highlighted for these two populations and for diverse kinds of mortar (Table 5), as also shown in Fig. 8b where the MT sample population has an evidently different behaviour with respect to HB mortars. Overall, the MT samples show lower values of open helium porosity and consequent greater values of bulk density, highlighting a higher compactness in the production of mortar and probably also a minor chemical-physical alteration degree (for dissolution and decohesion processes) of the binders. This trend is observed when also analysing the data within each group, especially for the brick and

Table 5

Physical properties of analysed mortars. Abbreviations: ρ_R = real density; ρ_B = bulk density; $\Phi_O He$ = helium open porosity; $\Phi_O H_2O$ = water open porosity; IC_W = water imbibition coefficient; SI = water saturation index; $Is_{(50)}$ = Point Load strength index; R_C = indirect compression strength; R_T = indirect traction strength; St. Dev. = standard deviation.

Sample	Mortar type	ρ_R	ρ_B	Φ_O (He)	Φ_O (H₂O)	IC_W	SI	$Is_{(50)}$	R_C	R_T
		(g/cm³)	(g/cm³)	(%)	(%)	(%)	(%)	(N/mm²)	(N/mm²)	(N/mm²)
ADTM 1a	Brick bedding mortars	2.69	1.80	33.2	30.7	17.0	92.2	2.36	33.03	2.95
ADTM 2		2.59	1.76	32.0	30.2	17.1	94.3	0.64	8.89	0.79
ADTM 4		2.57	1.45	43.7	41.4	28.6	94.7	0.44	6.18	0.55
ADTM 5		2.64	1.81	31.4	30.8	17.0	98.4	0.51	7.13	0.64
ADTM 6a		2.61	1.81	30.7	24.0	13.3	78.2	n.d.	n.d.	n.d.
ADTM 8a		2.65	1.57	40.6	38.3	24.3	94.3	0.10	1.46	0.13
ADTM 10		2.61	1.60	38.8	35.0	21.9	90.3	0.20	2.83	0.25
ADTM 11		2.62	1.57	40.0	39.3	24.9	98.2	0.09	1.31	0.12
Mean		2.62	1.67	36.3	33.7	20.5	92.6	0.62	8.69	0.78
St. Dev.		0.04	0.14	5.0	5.8	5.2	6.4	0.79	11.12	0.99
ADTM 3	*Cubilia* bedding mortars	2.49	1.60	35.7	33.1	20.6	92.6	1.97	27.53	2.46
ADTM 7		2.43	1.45	40.3	35.5	24.4	87.9	0.64	8.91	0.80
ADTM 14		2.62	1.44	45.2	40.1	27.8	88.6	0.97	13.55	1.21
ADTM 22		2.54	1.77	30.5	29.5	16.6	96.9	n.d.	n.d.	n.d.
ADTM 23		2.66	1.59	40.2	38.0	23.8	94.4	1.65	23.14	2.07
ADTM 25		2.46	1.45	41.0	37.5	25.7	91.4	0.99	13.83	1.23
Mean		2.54	1.55	38.8	35.6	23.2	92.0	1.24	17.39	1.55
St. Dev.		0.09	0.13	5.1	3.8	4.0	3.4	0.55	7.67	0.68
ADTM 24 ar	Renderings (*arriccio*)	2.52	1.42	43.5	40.5	28.3	92.9	0.50	7.00	0.63
ADTM 32 ar		2.58	1.39	46.1	41.9	30.1	90.9	n.d.	n.d.	n.d.
Mean		2.55	1.41	44.8	41.2	29.2	91.9	n.d.	n.d.	n.d.
St. Dev.		0.04	0.02	1.8	1.0	1.3	1.4	n.d.	n.d.	n.d.
ADTM 24 in	Setting coat plasters	2.50	1.28	48.6	45.2	35.1	93.0	n.d.	n.d.	n.d.
ADTM 25 in		2.55	1.47	42.2	36.6	24.8	86.8	n.d.	n.d.	n.d.
Mean		2.52	1.38	45.4	40.9	29.9	89.9	n.d.	n.d.	n.d.
St. Dev.		0.04	0.13	4.5	6.0	7.3	4.4	n.d.	n.d.	n.d.

cubilia bedding mortars, while the *arriccio* layer of MT renderings shows greater values of porosity and lower bulk density with respect to HB mortars with same function (Fig. 8; Table 5). The brick and *cubilia* bedding MT mortars (as well as HB mortars) also have lower values of porosity with respect to the wall coating mortars for the marble slabbing and to the conglomerate mortars coming from *Heliocaminus* Baths (Fig. 8). In the first case, this is due to the different function and in second case, to the different kinds of aggregate, mainly consisting of *cocciopesto* and other *lateritious* angular fragments [10,11] which normally increase the porosity of mortars.

The finishing layers (*i.e. intonachino*) of MT mortars show variable data (Table 5), with open helium porosity from about 42 to 48%. Due to these differences in the porosity, despite with lower values, the water open porosity follows the same physical behaviour. On the graphic of Fig. 8c, where helium open porosity *vs* water open porosity is reported, the mortars are positioned below the line of 100% water saturation.

Despite a lower open porosity, the MT mortar samples generally show greater saturation index values with respect to the HB mortars, probably due to different pore physical features of binders (*e.g.* radius, geometry, tortuosity).

Primarily, PLT mechanical strength of MT mortars reflects their different function in the building: the brick bedding mortars show higher values of punching index ($Is_{(50)}$) with respect to the *cubilia* bedding mortars (Table 5). These samples show even greater values with respect to HB mortars with the same technical function. Considering the similar composition of the aggregate in these two MT mortar groups, probably the greater PLT strength of brick mortars is due to the easy laying of elements in contrast to the *cubilia*; in fact, in the latter case, the laying does not allow a perfect filling of space with the mortar between the *cubilia* ashlars, due to their pyramidal shape.

Within each mortar group, the PLT mechanical strength depends on the porosity of the mortar (Table 5). The punching index shows

Table 6

Physical properties of analysed *cubilia* volcanic stones. Abbreviations: ρ_S = solid density; ρ_R = real density; ρ_B = bulk density; $\Phi_O He$ = helium open porosity; $\Phi_O H_2O$ = water open porosity; $\Phi_C He$ = helium closed porosity; IC_W = water imbibition coefficient; SI = water saturation index; $Is_{(50)}$ = Point Load strength index; R_C = indirect compression strength; R_T = indirect traction strength; St. Dev. = standard deviation.

Sample	ρ_S	ρ_R	ρ_B	Φ_O (He)	Φ_O (H₂O)	Φ_C (He)	Φ_o	IC_W	SI	$Is_{(50)}$	R_C	R_T
	(g/cm³)	(g/cm³)	(g/cm³)	(%)	(%)	(%)	(%)	(%)	(%)	(N/mm²)	(N/mm²)	(N/mm²)
ADTM1b	2.47	2.41	1.59	34.0	31.1	1.4	35.4	19.4	91.5	0.86	12.10	1.08
ADTM18b	2.48	2.45	1.63	33.4	30.9	0.7	34.1	18.9	92.6	0.34	4.72	0.42
ADTM27b	2.54	2.50	1.53	38.7	36.1	1.0	39.7	23.5	93.2	0.50	6.95	0.62
ADTM30	2.48	2.43	1.59	34.8	29.4	1.3	36.1	18.5	84.6	1.18	16.47	1.47
Mean	2.49	2.45	1.58	35.2	31.9	1.1	36.3	20.1	90.5	0.72	10.06	0.90
St. Dev.	0.03	0.04	0.04	2.4	2.9	0.3	2.4	2.3	4.0	0.38	5.27	0.47
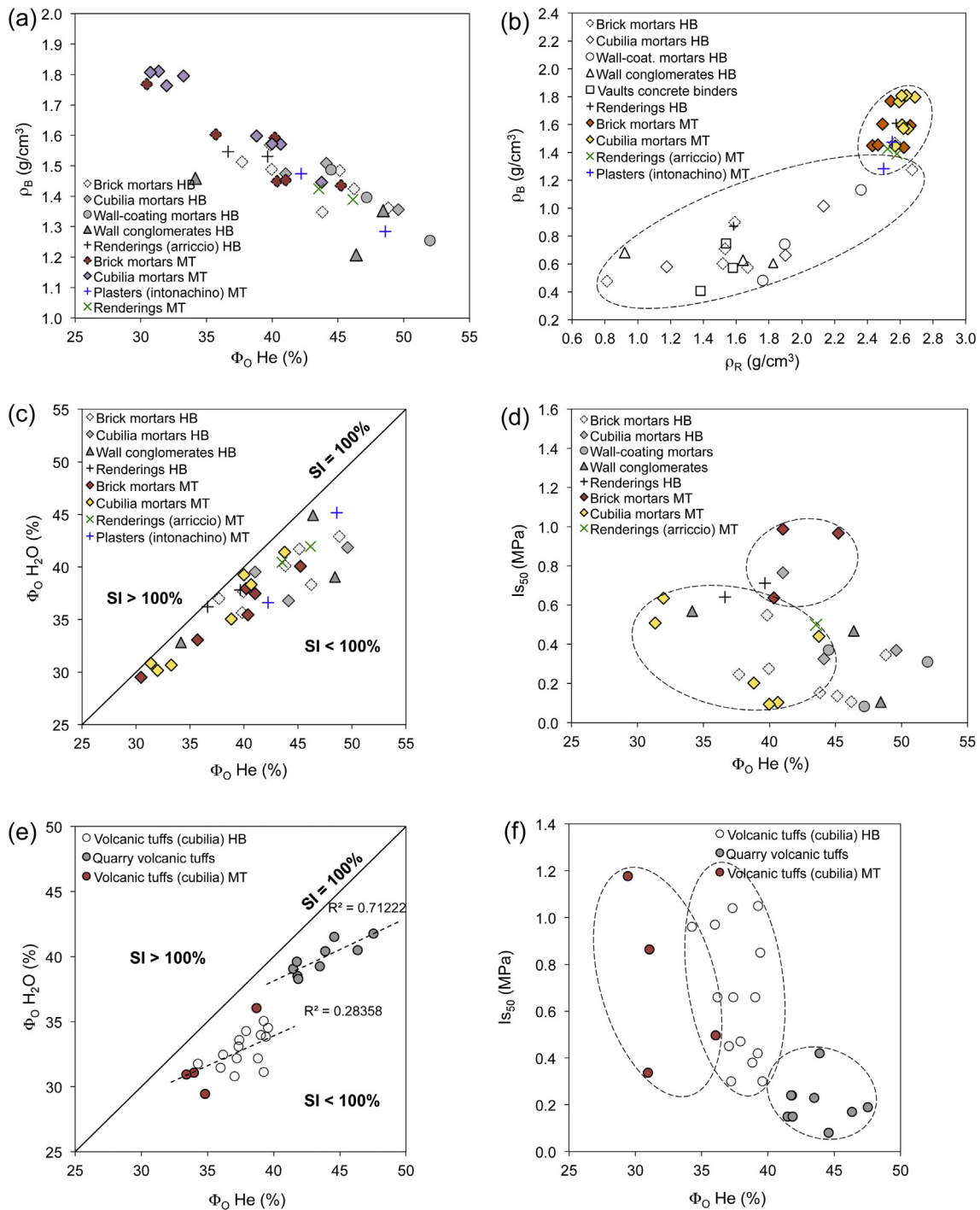
Fig. 8. Physical properties of mortars and *cubilia* stones from Maritime Theater (MT) mortars and, to make a comparison, from nearly *Heliocaminus* Baths building (HB): (a) He open porosity (Φ_O He) *vs* bulk density, divided in different groups of mortar typology; (b) bulk density *vs* real density, (c) helium open porosity *vs* water open porosity of mortars, (d) He open porosity (Φ_O He) *vs* punching strength of mortars, (e) helium open porosity *vs* water open porosity of *cubilia* pyroclastites, (f) He open porosity (Φ_O He) *vs* punching strength of *cubilia* pyroclastites.

exponential and polynomial negative correlations with helium open porosity, with R^2 coefficients of 0.38 and 0.58 in *cubilia* and brick mortars respectively (Fig. 8d).

In Fig. 8e and f are plotted data (reported in Table 6) of water open porosity *vs* helium open porosity and He-open porosity *vs* punching index of the samples taken from MT *cubilia* respectively. In the same graphs, for comparison, the samples taken from *Heliocaminus* Baths and from volcanic outcrops in the area surrounding Hadrian's Villa are plotted. The MT samples show a physical behaviour similar to those

coming from the HB monument, but with greater values of porosity (Table 6). The populations of samples from two MT and HB monuments show a similar trend in open porosity and saturation index (Fig. 8d), but they have different values compared to the samples taken from outcrops (Table 6; Fig. 8d). These latter show greater porosity and consequently lower bulk density than those of the *cubilia* samples, due to their higher alteration degree. In fact, the outcrop samples come from the most superficial portion of the rocky outcrop. In contrast, the *cubilia* samples belong to the "fresh" rocky outcrops of ancient quarries or several

source points within the Hadrian's Villa area. This different physical behaviour is also well highlighted by the PLT mechanical strength of these two populations (Table 6; Fig. 8f).

4. Conclusions

The results highlight that the ancient building of the Maritime Theatre respects the architectural and structural constructive technologies of Roman times. It was constructed with different materials: various kinds of brick, pyroclastic rocks (for *cubilia* ashlars) and other ornamental stones (typically marble) using hydraulic and lime mortars.

Volcanic rocks and crushed crystal- and litho-clasts were mainly used as aggregate in the mortars. *Cocciopesto* is rare or absent in the aggregate, and thus probably not intentionally incorporated. The volcanic aggregate consists of leucitic basalt scoria and leucitites. These rocks, together with the *cubilia* pyroclastics (outcropping within the Hadrian's Villa area), belong to the alkaline rocks of ultrapotassic series (HKS) from the Roman Magmatic Province.

Basalt scoria used as aggregate in the mortars reacts with the binder, while leucitite doesn't show reactivity, probably due to its high crystallinity and the almost total absence of glass in the matrix. Scoria, along with *cocciopesto* aggregates (although generally not used as the main aggregate), give good pozzolanic characteristics to the mortars of the Maritime Theatre, similar to those used for the adjacent *Heliocaminus* Baths.

The use of different raw materials in the production of mortars and mixing proportions of aggregates and binder are made according to the known Roman standard methods as suggested by *Vitruvio* [45], using different mixtures in relation to the mortar's function in the masonry.

The results of the mechanical tests highlight the low mechanical strength of the mortars that essentially depends on the high porosity of the analysed samples, due to evident chemical-physical decay processes – *i.e.* binder dissolution, hydration/dehydration/crystallization of hygroscopic minerals (gypsum, ettringite, etc.) – with the consequent decohesion, disintegration and mass loss of the mortar.

Raman spectroscopy on the only remains of original Roman microstratified paintings of wall plasters located under the vault have shown that the first inner reddish layer (corresponding to a first stage) mainly consists of hematite, while the outer second layer (corresponding to a later painting) consists of Egyptian Blue. That highlights the probable presence of two different phases of the Maritime Theatre wall decoration in Roman times.

Acknowledgements

References

[1] M. Üblacker, Das Teatro Marittimo in der Villa Hadriana, Philipp von Zabern, Mainz am Rhein, 1985.
[2] W.L. Mac Donald, J.A. Pinto, Villa Adriana: la costruzione e il mito da Adriano a Louis I. Kahn (trad. it.). Electa Architettura, Milano, 1997.
[3] A. Camiz, La cosiddetta "Roccabruna" ed il dies imperii, in: L. Basso Peressut, P.F. Caliari (Eds.), Environments, Villa Adriana, Milano, 2004, pp. 121–129.
[4] P. Lapuente, P. León, T. Nogales, H. Royo, M. Preite-Martinez, Ph Blanc, White sculptural materials from Villa Adriana: study of provenance, Tarragona, in: A. Gutiérrez Garcia, P. Lapuente, I. Rodà (Eds.), Interdisciplinary studies on Ancient Stone. Proceedings of the IX ASMOSIA Conference, 2012, pp. 364–375.
[5] M. De Franceschini, Villa Adriana: mosaici, pavimenti, edifici, "L'Erma" di Bretschneider, Roma, 1991.
[6] V. Vincenti, Pavimenti musivi e cementizi di Villa Adriana, Mosaici Antichi in Italia, Regione Quarta, Istituti Editoriali e Poligrafici Internazionali, Pisa – Roma, 2017.

[7] P. Verduchi, Le Terme con cosiddetto *Heliocaminus* a Villa Adriana, Quaderni dell'Istituto di Topografia Antica 8 (1975) 55–95.
[8] P. Cicerchia, Sul carattere distributivo delle terme con *Heliocaminus* di Villa Adriana, Xenia 9 (1985) 47–60.
[9] S. Columbu, F. Antonelli, M. Lezzerini, D. Miriello, B. Adembri, A. Blanco, Provenance of marbles used in the *Heliocaminus* Baths of Hadrian's Villa (Tivoli, Italy), J. Archaeol. Sci. 49 (2014) 332–342.
[10] S. Columbu, F. Sitzia, G. Verdiani, Contribution of petrophysical analysis and 3D digital survey in the archaeometric investigations of the Emperor Hadrian's Baths (Tivoli, Italy), Rend. Fis Acc. Lincei, No. 26 (2015) 455–474.
[11] S. Columbu, F. Sitzia, G. Ennas, The ancient pozzolanic mortars and concretes of *Heliocaminus* baths in Hadrian's Villa (Tivoli, Italy), Archaeol. Anthropol. Sci. (2016), http://dx.doi.org/10.1007/s12520-016- 0385-1.
[12] P. Pensabene, F. Antonelli, L. Lazzarini, S. Cancelliere, Provenance of marble sculptures and artifacts from the so-called Canopus and other buildings of "Villa Adriana" (Hadrian's Villa, Tivoli, Italy), J. Archaeol. Sci. 39 (2012) 1331–1337.
[13] D. Attanasio, M. Bruno, W. Prochaska, A.B. Yavuz, The Asiatic marbles of the Hadrian's Villa at Tivoli, J. Archaeol. Sci. 40 (2013) 4358–4368.
[14] D. Attanasio, G. Mesolella, P. Pensabene, R. Platania, P. Rocchi, EPR and petrographic provenance of the architectural white marbles of three buildings at Villa Adriana, in: Y. Maniatis (Ed.), Asmosia VII. Proceeding 7th International Conference ASMOSIA, Thassos 2003, Bulletin de Correspondance Hellenique Sup., 51, Athens, 2009, pp. 57–369.
[15] J.P. Adam, L'arte di costruire presso i Romani, materiali e tecniche, Longanesi, 2006.
[16] F. Giuliani Cairoli, L'edilizia nell'antichità, Carocci, Roma, 2006.
[17] C. Stanislao, C. Rispoli, G. Vola, P. Cappelletti, V. Morra, M. De Gennaro, Contribution to the knowledge of ancient Roman seawater concretes: phlegrean pozzolan adopted in the construction of the harbour at Soli-Pompeiopolis (Mersin, Turkey), Periodico di Mineralogia 80 (3) (2011) 471–488.
[18] G. Vola, E. Gotti, C. Brandon, J.P. Oleson, R.L. Hohlfelder, Chemical, mineralogical and petrographic characterization of Roman ancient hydraulic concretes cores from Santa Liberata, Italy, and Caesarea Palestinae, Israel, Periodico di Mineralogia 80 (2) (2011) 317–338.
[19] D. Miriello, D. Barca, A. Bloise, A. Ciarallo, G.M. Crisci, T. De Rose, C. Gattuso, F. Gazineo, F. La Russa, Characterisation of archaeological mortars from Pompeii (Campania, Italy) and identification of construction phases by compositional data analysis, J. Archaeol. Sci. 37 (2010) 2207–2223.
[20] D. Miriello, A. Bloise, G.M. Crisci, C. Apollaro, A. La Marca, Characterization of archeological mortars and plasters from Kyme (Turkey), J. Archeol. Sci. 38 (2011) 794–804.
[21] S. Columbu, A.M. Garau, Mineralogical, petrographic and chemical analysis of geomaterials used in the mortars of Roman Nora theatre (south Sardinia, Italy), Italian J. Geosci. 136 (2017) 238–262.
[22] D. Miriello, F. Antonelli, C. Apollaro, A. Bloise, N. Bruno, E. Catalano, S. Columbu, G.M. Crisci, R. De Luca, M. Lezzerini, S. Mancuso, A. La Marca, New data about the ancient mortars from the archaeological site of Kyme (Turkey): compositional characterization, Per. Mineral. 84 (2015) 497–517.
[23] M. Drdácky, F. Fratini, D. Frankeová, Z. Slíz̆ková, The Roman mortars used in the construction of the Ponte di Augusto (Narni, Italy) a comprehensive assessment, Constr. Build. Mater. 38 (2013) 1117–1128.
[24] F. Antonelli, S. Columbu, M. Lezzerini, D. Miriello, Petrographic characterization and provenance determination of the white marbles used in the Roman sculptures of Forum Sempronii (Fossombrone, Marche, Italy), Appl. Phys. A 115 (2013) 1033–1040.
[25] F. Antonelli, S. Columbu, Raaijmakers M. De Vos, M. Andreoli, An archaeometric contribution to the study of ancient millstones from the Mulargia area (Sardinia, Italy) through new analytical data on volcanic raw material and archaeological items from Hellenistic and Roman North Africa, J. Archaeol. Sci. 50 (2014) 243–261.
[26] S. Columbu, A. Gioncada, M. Lezzerini, M. Marchi, Hydric dilatation of ignimbritic stones used in the church of Santa Maria di Otti (Oschiri, northern Sardinia, Italy), Ital. J. Geosci. 133 (2014) 149–160.
[27] P. Maravelaki-Kalaitzaki, A. Bakolas, A. Moropoulou, Physico-chemical study of Cretan ancient mortars, Cem. Concr. Res. 33 (2003) 65 61.
[28] A. Moropoulou, A. Bakolas, K. Bisbikou, Investigation of the technology of historic mortars, J. Cult. Heritage 1 (2000) 45–58.
[29] P. Smith, R.M. Smith, Bricks and mortar: a method for identifying construction phases in multistage structures, Histor. Archaeol. 43 (2009) 40–60.
[30] I.B. Topçu, B. Isıkdag, The effect of ground granulated blast-furnaceslag on properties of Horasan mortar Burak Iβsıkdag, Constr. Build. Mater. 40 (2013) 448–454.
[31] G. Bertorino, M. Franceschelli, M. Marchi, C. Luglié, S. Columbu, Petrographic characterisation of polished stone axes from Neolithic Sardinia, archaeological implications, Per. Mineral. 71 (2002) 87–100.
[32] P. Adriano, A. Santos Silva, R. Veiga, J. Mirão, A.E. Candeias, Microscopic characterization of old mortars from Santa Maria Church in Énvora, Mater. Charact. 60 (7) (2009) 610–620.
[33] S. Columbu, G. Verdiani, Digital survey and material analysis strategies for documenting, monitoring and study the Romanesque Churches in Sardinia, Italy, Lecture Notes in Computer Science, Springer, 2014, pp. 446–453.
[34] G. Verdiani, S. Columbu, E. Stone, An archive for the Sardinia monumental witnesses, Lecture Notes Comput. Sci. 6436 (2010) 356–372.
[35] S. Columbu, Provenance and alteration of pyroclastic rocks from the Romanesque Churches of Logudoro (north Sardinia, Italy) using a petrographic and geochemical statistical approach, Appl. Phys. A: Mater. Sci. Process. 123 (3) (2017) 165.
[36] A. Moropoulou, K. Polikreti, A. Bakolas, P. Michailidis, Correlation of

physicochemical and mechanical properties oh historical mortars and classification by multivariate statistics, Cem. Concr. Res. 33 (2003) 891–898.

[37] M. Lezzerini, F. Antonelli, S. Columbu, R. Gadducci, A. Marradi, D. Miriello, L. Parodi, L. Secchiari, A. Lazzeri, The documentation and conservation of the cultural heritage: 3D laser scanning and gis techniques for thematic mapping of the stonework of the Façade of St. Nicholas Church (Pisa, Italy), Int. J. Architect. Heritage: Conserv. Anal. Restor. 10 (1) (2016) 9–19.

[38] L.A. Ortega, M.C. Zuluaga, A. Olazabal, Geochemical characterization of archaeological lime mortars: provenance inputs, Archaeometry 50 (3) (2008) 387–408.

[39] G. Macciotta, G. Bertorino, A. Caredda, S. Columbu, R. Coroneo, M. Franceschelli, M. Marchi, S. Rescic, The S.Antioco of Bisarcio Basilica (NE Sardinia, Italy): water-rock interaction in ignimbrite monument decay, Cidu Ed. Water-Rock Interaction (WRI-10), Swets and Zeitlinger, Lisse, 2001, pp. 415–418.

[40] S. Columbu, G. Cruciani, D. Fancello, M. Franceschelli, Musumeci, Petrophysical properties of a granite-protomylonite-ultramylonite sequence: insight from the

Monte Grighini shear zone, central Sardinia, Italy, Eur. J. Mineral. 27 (4) (2015) 471–486.

[41] ISRM, International Society for Rock Mechanics, Suggest method for determining the point load strength index. ISRM (Lisbon, Portugal). Committee on field tests. Document n.1, 1972, pp. 8–12.

[42] ISRM, International Society For Rock Mechanics, Suggest method for determining the point load strength. ISRM commis- sion for testing methods, Working group on revision of the point load, 1985.

[43] A. Palmstrom, RMi-A rock mass characterization system for rock engineering purposes, Ph D. thesis University of Oslo, Norway, 1995.

[44] A. Peccerillo, Plio-Quaternary volcanism in Italy, Petrology, Geochemistry, Geodynamics, Springer, Heidelberg, 2005.

[45] Pollione MV (15 BC) De Architecture. Vol. II. In: Cesariano C, De Architectura Libri Dece, 1521, Como.